J. Fluid Mech. (1992), *vol.* 244, *pp.* 307–322

The squeezing of red blood cells through parallel-sided channels with near-minimal widths

By D. HALPERN[1] AND T. W. SECOMB[2]

[1] Department of Biomedical Engineering, Northwestern University, Evanston, IL 60208, USA
[2] Department of Physiology, University of Arizona, Tucson, AZ 85724, USA

(Received 5 August 1991 and in revised form 16 March 1992)

An analysis of the motion and deformation of red blood cells between two parallel flat plates is presented. The motion is driven by an imposed pressure gradient in the surrounding fluid. Mammalian red cells are highly flexible, but deform at constant volume because the contents of the cell are incompressible, and at nearly constant surface area because the membrane strongly resists dilatation. Consequently, a minimum spacing between the plates exists, below which passage of intact cells is not possible. We consider spacings slightly larger than this minimum. The shape of the cell in this case is a disk with a rounded edge. The flow of the surrounding fluid is described using lubrication theory. Under the approximation that the distance between the plates is small compared with the cell diameter, cell shapes, pressure distributions, membrane stresses and cell velocities are deduced as functions of geometrical parameters. It is found that the narrow gaps between the cell and the plate are not uniform in width, and that as a result, membrane shear stresses are generated which increase in proportion to flow velocity. This contrasts with axisymmetric configurations, in which membrane shear stress remains bounded as cell velocity increases. The variation of cell velocity with spacing of the plates is similar to that previously demonstrated for rigid disk-shaped particles of corresponding dimensions.

1. Introduction

The aim of this paper is to analyse the motion and deformation of a tightly fitting red blood cell between two parallel plates, driven by a pressure gradient in the fluid surrounding the cell.

Mechanical properties of mammalian red blood cells have been determined experimentally. A thin, highly flexible, viscoelastic membrane surrounds a Newtonian fluid. The membrane strongly resists area changes, having a large isotropic modulus, and so red cells deform at constant volume and almost constant surface area (Canham & Burton 1968). As a result, there are lower bounds on the dimensions of passages that will permit passage of intact red cells. For typical human red blood cells, with area 135 μm^2 and volume 90 μm^3, a cylindrical tube must be at least 2.84 μm in diameter for cell passage. Halpern & Secomb (1989) analysed the mechanics and motion of cells in tubes with diameters slightly larger than this.

Most theoretical studies of red blood cell motion in the microcirculation have assumed that microvessels are approximately cylindrical. However, red cells in the microcirculation must also traverse passages with non-axisymmetric geometries. Such passages may have near-minimal dimensions. For example, microvessels that

participate in blood flow regulation are able to constrict strongly, to the extent that red cell motion is obstructed, and the remaining passage is highly non-circular (Greensmith & Duling 1984). In the spleen, red blood cells pass through narrow slits between cells comprising the walls of venous sinuses (Drenckhahn & Wagner 1986). In the lung, the pulmonary capillaries may be modelled as a space between parallel plates, whose width may decrease to near zero at low capillary pressures (see Fung 1990, p. 209). The geometry considered in this analysis is much simpler than those encountered by red cells in the above examples, but retains two important features. Firstly, the stresses acting on the cell are strongly non-axisymmetric. Secondly, the cell does not nearly fill the entire passage, as it does in a cylindrical tube with near-minimal diameter, and so the suspending fluid may flow around the cell, even if the cell velocity is small.

For a red cell with the dimensions quoted above, the minimum spacing between two plates which permits passage of intact cells is 1.82 μm. The shape of a cell squeezed between two plates with this spacing (the critical shape) is a disk with a rounded edge (Halpern 1989), of overall diameter 8.32 μm. The profile of the rim is then very nearly a semicircle and we shall use this approximation here. We consider the case in which the distance between the plates is slightly larger than the minimum spacing, which we refer to as the near-critical case. The cell shape is then close to the critical shape, and the gap between the cell and the plates is much smaller than the distance between the plates. This distance is itself much smaller than the cell diameter (by a factor of about five for the dimensions quoted above).

The analogous problem for a rigid particle with the critical shape has been analysed by Halpern & Secomb (1991). Here, we emphasize aspects of the problem relating to cell deformability. In §2, equations of membrane equilibrium and lubrication equations for the fluid flow around the cell are established. These equations are solved in §§3 and 4, yielding estimates for fluid and cell velocities, cell shape and membrane deformation in the almost-planar region.

2. Governing equations

2.1. *Geometry and boundary conditions*

The flow geometry is indicated in figure 1. Cylindrical coordinates (r, θ, z) and Cartesian coordinates (x, y, z), moving with the cell, are used. Points on the membrane are identified in terms of θ and s, the arclength measured from the axis. On the curved rim, ϕ is the angle between the membrane and the plates. We assume that the cell has mirror symmetry with respect to the midplane of the channel, $z = \frac{1}{2}d$, and with respect to the plane $y = 0$. The membrane adjacent to the lower plate is located at $z = h(r, \theta)$. The flow domain is divided into three regions:

region I (the flat-disk region): $0 \leqslant r \leqslant r_1$, $h = h(r, \theta) \ll d$;

region II (the curved rim): $r_1 \leqslant r \leqslant r_2$, $h = h(r, \theta) \leqslant \frac{1}{2}d$;

region III (outside the disk): $r \geqslant r_2$, $h = d$.

Note that the gap width h jumps from $\frac{1}{2}d$ to d between region II and region III.

We consider the case in which the entire cell travels with a uniform velocity, i.e. the membrane does not move relative to the cell. Transient membrane deformations may occur when the cell enters the channel (see §4). The formulation here applies to steady configurations. Then $\boldsymbol{u} = (u_r, u_\theta, u_z) = 0$ on the surface of the cell (regions I and II). We assume that the cell is moving with speed u_1 in the $\theta = \pi$ direction relative to the plates. Therefore, in the particle frame, $\boldsymbol{u} = u_1 \boldsymbol{i}_x$ on the plates ($z = 0$, $z = d$), where $\boldsymbol{i}_x = (\cos\theta, -\sin\theta, 0)$ is the unit vector in the $\theta = 0$ direction. Far from

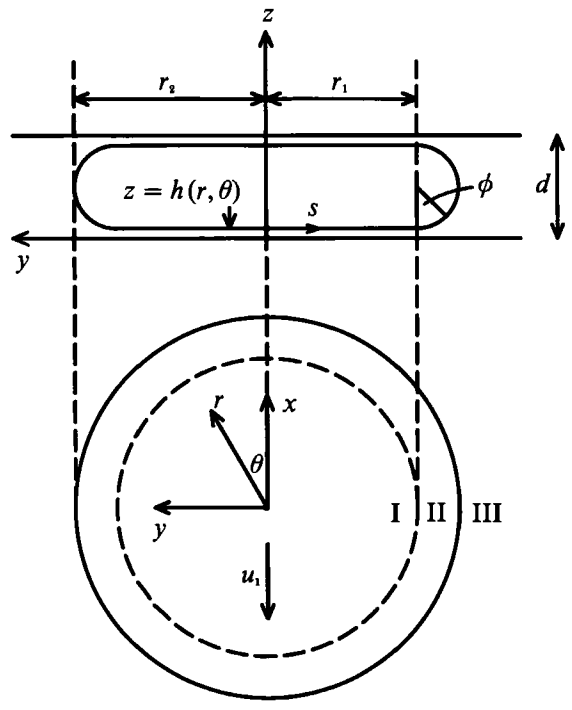

FIGURE 1. Variables used to describe geometry of critical cell between two parallel plates, and regions used in analysis.

the cell, the flow approaches unidirectional plane Poiseuille flow, with mean velocity u_2 in the $\theta = \pi$ direction relative to the plates. Therefore $\bar{\boldsymbol{u}} \to (u_1 - u_2)\, \boldsymbol{i}_x$ in the particle frame as $r \to \infty$, where $\bar{\boldsymbol{u}}$ is the z-average of $\boldsymbol{u}$.

2.2. *Membrane equilibrium*

The equations of membrane equilibrium in the radial and azimuthal directions are (Timoshenko & Woinowsky-Krieger 1959):

$$\frac{1}{r}\frac{\partial}{\partial s}(rt_{ss}) + \frac{1}{r}\frac{\partial t_{s\theta}}{\partial \theta} - \frac{\cos\phi}{r} t_{\theta\theta} = -\tau_r, \tag{2.1}$$

and

$$\frac{1}{r}\frac{\partial t_{\theta\theta}}{\partial \theta} + \frac{1}{r}\frac{\partial}{\partial s}(rt_{s\theta}) + \frac{\cos\phi}{r} t_{s\theta} = -\tau_\theta, \tag{2.2}$$

where t_{ss}, $t_{\theta\theta}$ and $t_{s\theta}$ are components of membrane stress and τ_r and τ_θ are external shear stresses. The equation for equilibrium of normal stress is

$$\frac{\partial \phi}{\partial s} t_{ss} + \frac{\sin\phi}{r} t_{\theta\theta} = -(p - p_1), \tag{2.3}$$

where p_1 and p are the internal and external pressures. Since there is no relative internal motion of the cell, the internal pressure is a constant. The external stresses depend on the flow of the surrounding fluid.

To complete the specification of the problem, constitutive relations for the membrane are required. We postpone introducing these until §4, and compute membrane stresses assuming that they can be achieved by suitable membrane strains.

2.3. *Flow of surrounding fluid*

The flow of the suspending fluid satisfies the Stokes equations. The narrowness of the gaps between the cell and the plates suggests the use of lubrication theory. We use lubrication equations to describe the flow throughout regions I and II. At the outer edge of region II, the gap is no longer narrow relative to the radial lengthscale. However, Halpern & Secomb (1991) have argued that the lubrication equations still yield a good approximation in this region. The essential point is that the pressure gradient decays rapidly as the gap widens, so that errors in describing the flow in the regions of wider gap have little effect on the overall pressure field.

We also use lubrication equations in region III, leading to a Hele-Shaw flow problem. This approximation is based on the assumption that the distance between the plates is much smaller than the radial and azimuthal lengthscales. For typical human red cells, the ratio of cell width to cell diameter is about 0.22, suggesting that this assumption will yield a useful approximation overall. However, the assumption breaks down in a 'boundary layer' of width $O(d)$ surrounding the cell (Halpern & Secomb 1991). The effect of the boundary layer on the external pressure field and on the cell velocity is equivalent to that of increasing the cell radius by a 'displacement thickness' of about $0.3d$, and is not included here.

According to the assumptions of lubrication theory, u_z is negligible and pressure is independent of z. We non-dimensionalize as follows:

$$\left.\begin{gathered} R=\frac{r}{d},\quad X=\frac{x}{d},\quad Y=\frac{y}{d},\quad Z=\frac{z}{d},\quad S=\frac{s}{d},\quad H=\frac{h}{d},\quad U_{\mathrm{p}}=\frac{u_1}{u_2}, \\ \boldsymbol{U}(R,\theta,Z)=(U_R,U_\theta,0)=\frac{\boldsymbol{u}(r,\theta,z)}{u_2},\quad P(R,\theta)=\frac{[p(r,\theta)-p_i]d}{12\mu u_2} \end{gathered}\right\} \tag{2.4}$$

(the factor of 12 simplifies subsequent expressions). Then the momentum and continuity equations are

$$12\nabla P=\frac{\partial^2 \boldsymbol{U}}{\partial Z^2},\quad \nabla\cdot\boldsymbol{U}=0, \tag{2.5}$$

and the boundary conditions are

$$\boldsymbol{U}=U_{\mathrm{p}}\boldsymbol{i}_x \quad \text{at} \quad Z=0,\quad \boldsymbol{U}=kU_{\mathrm{p}}\boldsymbol{i}_x \quad \text{at} \quad Z=H \quad \text{and} \quad \bar{\boldsymbol{U}}\to(U_{\mathrm{p}}-1)\boldsymbol{i}_x \quad \text{as} \quad R\to\infty, \tag{2.6}$$

where $k=0$ in regions I and II and $k=1$ in region III.

The momentum equation may be integrated, yielding

$$\boldsymbol{U}=6Z(Z-H)\nabla P+U_{\mathrm{p}}\left(1-(1-k)\frac{Z}{H}\right)\boldsymbol{i}_x. \tag{2.7}$$

Next, we define the flow rate

$$\boldsymbol{Q}=(Q_R,Q_\theta)=\int_0^H \boldsymbol{U}\,\mathrm{d}Z=-H^3\nabla P+\tfrac{1}{2}H(1+k)\,U_{\mathrm{p}}\boldsymbol{i}_x. \tag{2.8}$$

The continuity equation implies that $\nabla\cdot\boldsymbol{Q}=0$, that is

$$\nabla\cdot(H^3\nabla P)=\tfrac{1}{2}U_{\mathrm{p}}(1+\mathrm{k})\boldsymbol{i}_x\cdot\nabla H, \tag{2.9}$$

or

$$\frac{1}{R}\frac{\partial}{\partial R}\left(RH^3\frac{\partial P}{\partial R}\right)+\frac{1}{R^2}\frac{\partial}{\partial\theta}\left(H^3\frac{\partial P}{\partial\theta}\right)=\tfrac{1}{2}(1+k)U_{\mathrm{p}}\left(\cos\theta\frac{\partial H}{\partial R}-\frac{\sin\theta}{R}\frac{\partial H}{\partial\theta}\right). \tag{2.10}$$

3. Cell shape and motion

The equations derived in §2 are solved in regions I, II and III, and the solutions are matched at the boundaries between regions.

3.1. *Matching conditions*

Matching conditions in the fluid are as for rigid particles (Halpern & Secomb 1991), namely continuity of pressure and radial flow rate. The membrane stress component t_{ss} is continuous at $R = R_1 = r_1/d$. At $R = R_2 = r_2/d$, the total curvature of the rim is approximately 2, since the rim profile is approximately semicircular with radius $\frac{1}{2}$, and the curvature in the azimuthal direction is relatively small. Hence

$$P^{\mathrm{I}} = P^{\mathrm{II}}, \quad Q_R^{\mathrm{I}} = Q_R^{\mathrm{II}}, \quad T_S^{\mathrm{I}} = T_S^{\mathrm{II}} \quad \text{at} \quad R = R_1; \tag{3.1}$$

$$P^{\mathrm{II}} = P^{\mathrm{III}}, \quad 2Q_R^{\mathrm{II}} = Q_R^{\mathrm{III}}, \quad 2T_S^{\mathrm{II}} = -P^{\mathrm{III}} \quad \text{at} \quad R = R_2, \tag{3.2}$$

where $T_S = t_{ss}/(12\mu u_2)$ and the last condition follows from (2.3). Continuity of tangential flow rate cannot be imposed under the assumptions of §2, unless the 'boundary layer' around the cell is included (Halpern & Secomb 1991).

3.2. *Region I*

In the case of a closely fitting rigid particle, Halpern & Secomb (1991) showed that the pressure gradient in region I becomes large if the gap is very narrow. For a flexible cell, in contrast, the following argument shows that the pressure gradient in region I must be small.

Estimates of membrane curvatures, K^{I} and K^{II}, in regions I and II are

$$K^{\mathrm{I}} = O(H_{\mathrm{m}}/R_1^2) \ll 1, \quad K^{\mathrm{II}} \approx 2, \tag{3.3}$$

where H_{m} is the mean gap width in region I. In the near-critical case, we expect that the membrane is under tension over its entire surface (cf. Halpern & Secomb 1989). Let $12\mu u_2 T_{\mathrm{m}}$ be an estimate of the tension. Then the pressure differences, P^{I} and P^{II}, across the membrane in regions I and II are

$$P^{\mathrm{I}} = O(H_{\mathrm{m}} T_{\mathrm{m}}/R_1^2), \quad P^{\mathrm{II}} = O(T_{\mathrm{m}}). \tag{3.4}$$

Clearly $P^{\mathrm{I}} \ll P^{\mathrm{II}}$, and therefore $P^{\mathrm{I}} = 0$ at leading order. From (2.9), it follows that

$$H = H(R\sin\theta) = H(Y) \tag{3.5}$$

in region I, i.e. the gap width is uniform in region I along lines parallel to the flow direction. The radial flow rate is then

$$Q_R^{\mathrm{I}} = \tfrac{1}{2} H U_{\mathrm{p}} \cos\theta. \tag{3.6}$$

3.3. *Region II*

The governing equations for region II are obtained by combining the equations of membrane equilibrium with those of lubrication theory, from §2. Under the assumption that the cell thickness, and hence the width of region II, is small compared to the cell diameter, (2.10) may be approximated by

$$\frac{\partial}{\partial R}\left(H^3 \frac{\partial P^{\mathrm{II}}}{\partial R}\right) = \tfrac{1}{2} U_{\mathrm{p}} \cos\theta \frac{\partial H}{\partial R}. \tag{3.7}$$

Halpern (1989) showed that this approximation introduces a small error for rigid particles with typical cell dimensions. Near $\theta = \frac{1}{2}\pi$, $\cos\theta$ is small, and this

approximation may lead to unrealistic results, as discussed in §3.4 below. Equation (3.7) may be integrated:

$$\frac{\partial P^{\mathrm{II}}}{\partial R} = \tfrac{1}{2}H^{-2}U_p\cos\theta - K_2(\theta)H^{-3}, \tag{3.8}$$

where

$$K_2(\theta) = Q_R^{\mathrm{II}} \tag{3.9}$$

from (2.8), and so the radial flow rate is independent of R in this approximation.

We use the same approximation to simplify the equations of membrane equilibrium, by neglecting derivatives and curvatures in the azimuthal direction. Also, since the rim is relatively narrow, (2.1) shows that variations of T_s with R are relatively small, i.e. $T_s = T_s(\theta)$. Equation (2.3) reduces to

$$T_s\frac{\partial\phi}{\partial S} = -P. \tag{3.10}$$

This is combined with the equations of lubrication theory to yield

$$\partial H/\partial S = \sin\phi, \tag{3.11}$$

$$\partial\phi/\partial S = -P/T_S, \tag{3.12}$$

$$\partial P/\partial S = \tfrac{1}{2}U_{\mathrm{p}}\cos\theta(H^{-2} - H_1H^{-3}), \tag{3.13}$$

where $H_1(\theta) = H(R_1\sin\theta)$ is the gap width at $R = R_1$, and (3.11) follows from geometry. These equations are similar to those derived for the motion of axisymmetric red blood cells in cylindrical tubes (Halpern & Secomb 1989), and the same type of analysis can be performed here since θ can be treated as a parameter.

3.4 *The transition region*

Between regions I and II, curvature and, from (3.10), pressure change abruptly. Therefore, the solutions in regions I and II must be matched through a narrow transition region (cf. Secomb *et al.* 1986; Halpern & Secomb 1989). The scalings in this transition region depend on the local gap width $H_1(\theta)$ at the edge of region I. We seek solutions in which the variations of ϕ are small, and introduce the following scalings:

$$H = H_1H_{\mathrm{t}}, \quad S - R_1 = H_1^{\alpha_1}S_{\mathrm{t}}, \quad P = \tfrac{1}{12}H_1^{\alpha_2}P_{\mathrm{t}}, \quad T_{\mathrm{S}} = \tfrac{1}{12}H_1^{\alpha_3}T_{\mathrm{t}}, \quad \phi = H_1^{\alpha_4}\phi_{\mathrm{t}}, \tag{3.14}$$

where S_{t} (the independent variable) and H_{t}, P_{t}, T_{t}, ϕ_{t} are all $O(1)$ in the transition region, provided $\cos\theta$ is not small. For matching with region II, the curvature $\mathrm{d}\phi/\mathrm{d}S$ is $O(1)$, and so $\alpha_1 = \alpha_4$. The viscous drag on the particle in region I varies inversely with the gap width in the limit of narrow gap, while the driving pressure around the edge of the cell is independent of gap width in this limit. It follows from the zero-drag condition that U_{p} is proportional to the mean gap width in the limit of small gaps, so we let $U_{\mathrm{p}} = H_1(\theta)U_{\mathrm{t}}(\theta)$. The zero-drag condition is considered in more detail in §3.6. If the above scalings are substituted into (3.11)–(3.13), and powers of H_1 are equated, then it is found that $\alpha_1 = \alpha_4 = \frac{1}{2}$ and $\alpha_2 = \alpha_3 = -\frac{1}{2}$. The following system is obtained at leading order in the transition region

$$\partial H_{\mathrm{t}}/\partial S_{\mathrm{t}} = \phi_{\mathrm{t}}, \tag{3.15}$$

$$\partial\phi_{\mathrm{t}}/\partial S_{\mathrm{t}} = -P_{\mathrm{t}}/T_{\mathrm{t}} \tag{3.16}$$

$$\partial P_{\mathrm{t}}/\partial S_{\mathrm{t}} = 6\cos\theta\, U_{\mathrm{t}}(H_{\mathrm{t}}^{-2} - H_{\mathrm{t}}^{-3}). \tag{3.17}$$

The tension T_t is eliminated by introducing a new independent variable η_j:

$$\eta_j = \Gamma(S_t - S_{tm}), \quad H_t = f_j(\eta_j), \tag{3.18}$$

where

$$\Gamma^3 = \cos\theta\, U_t / T_t \tag{3.19}$$

For convenience, S_{tm} is chosen so $H_t = \frac{3}{2}$ when $S_t = S_{tm}$. Also, we distinguish between the leading the trailing edges of the cell by setting $j = 1$ at the leading edge ($\frac{1}{2}\pi < |\theta| < \pi$) and $j = 2$ at the trailing edge ($|\theta| < \frac{1}{2}\pi$), since Γ changes sign at $\theta = \pm\frac{1}{2}\pi$.

Substituting the new variables into (3.15)–(3.17), we obtain

$$f_j''' = 6(f_j^{-3} - f_j^{-2}), \tag{3.20}$$

where $f_j' = \partial f_j / \partial \eta_j$ and $f_j(0) = \frac{3}{2}$. For matching with region I,

$$f_1' \to 0 \quad \text{as} \quad \eta_1 \to \infty \quad \text{and} \quad f_2' \to 0 \quad \text{as} \quad \eta_2 \to -\infty. \tag{3.21}$$

Linearizing (3.21) about $f_j = 1$ gives two growing oscillatory solutions and one decaying monotonic solution in the positive η_j direction. It follows that in the transition adjacent to the leading edge, f_1 is uniquely determined, whilst at the trailing edge a one-parameter family of solutions exist. Numerical integration of (3.20) shows that

$$f_1'' \to k_1 \approx 2.123 \quad \text{as} \quad \eta_1 \to -\infty. \tag{3.22}$$

From (3.15) and (3.16), it follows that pressure in the gap and membrane curvature rapidly approach values independent of S in region II beyond the transition region. For matching with region III, the pressure is $P^{III}(R_2, \theta)$. From (3.2), (3.12), (3.14) and (3.18) we deduce that

$$k_1 \Gamma^2 = \frac{\partial \phi}{\partial S} = -P^{III}(R_2, \theta)/T_S(\theta) = 2 \tag{3.23}$$

in region II.

When Γ is written in terms of the original variables, (3.23) yields an expression for the gap width at the leading boundary of region I:

$$H_1(\theta) = -\frac{k_1}{2}\left|\frac{U_p \cos\theta}{12 T_S(\theta)}\right|^{\frac{2}{3}} = \frac{k_1}{2}\left|\frac{U_p \cos\theta}{6P^{III}(R_2, \theta)}\right|^{\frac{2}{3}} \tag{3.24}$$

for $\frac{1}{2}\pi < |\theta| < \pi$. This analysis shows that the gap width at the boundary between regions I and II in the leading part of the cell is determined by the interaction between fluid and membrane mechanics in the transition region, and depends on the local pressure difference across the membrane. According to (3.5), the gap width throughout region I is determined by the condition that $H(R_1 \sin\theta) = H_1(\theta)$, i.e. the gap width is everywhere equal to the gap width at the corresponding point (same Y-coordinate) at the leading edge of region I. At the trailing edge of region I, (3.5) implies that

$$H_1(\theta) = H_1(\pi - |\theta|) \quad \text{for} \quad |\theta| < \tfrac{1}{2}\pi. \tag{3.25}$$

This provides the additional boundary condition which determines uniquely the solution f_2 to (3.20). Since f_2 has oscillatory behaviour, the membrane bulges outwards slightly in the transition region at the trailing edge (Halpern & Secomb 1989).

According to (3.24), the gap width H_1 approaches zero as $\theta \to \pm\frac{1}{2}\pi$. This unrealistic behaviour occurs because the two-dimensional approximation used to obtain (3.7) is not uniformly valid near these points. To model this, an inner solution could be

obtained in the neighbourhood of $\theta = \pm\frac{1}{2}\pi$. However, this region contributes little to parameters such as the total shear force on the particle, and so we omit such an analysis.

3.5. *Region III*

In region III, $H = 1$ and the pressure equation (2.10) reduces to Laplace's equation

$$\frac{1}{R}\frac{\partial}{\partial R}\left(R\frac{\partial P}{\partial R}\right)+\frac{1}{R^2}\frac{\partial^2 P}{\partial \theta^2} = 0. \tag{3.26}$$

The general solution with the required symmetry is given by

$$P^{\mathrm{III}}(R,\theta) = P_0+R\cos\theta+\sum_{n=1}^{\infty} R^{-(2n-1)}a_n\cos(2n-1)\theta, \tag{3.27}$$

where the condition of plane Poiseuille flow at infinity has been applied. The radial flow rate is obtained from (2.8):

$$Q_R^{\mathrm{III}} = (U_{\mathrm{p}}-1)\cos\theta = \sum_{n=1}^{\infty}(2n-1)R^{-2n}a_n\cos(2n-1)\theta. \tag{3.28}$$

Applying the matching condition (3.1) to (3.6) and (3.9), we obtain

$$Q_R^{\mathrm{III}}(R_2,\theta) = 2K_2(\theta) = U_{\mathrm{p}}H_1(\theta)\cos\theta. \tag{3.29}$$

3.6. *The zero-drag condition*

Since inertial and buoyancy effects are negligible, the total fluid force on the cell is zero. By symmetry, only forces in the flow direction need to be considered. If $\mu u_2 dF_p$ is the pressure force and $\mu u_2 dF_\tau$ is the shear force on a cylindrical control volume surrounding the cell, then

$$F_\tau+F_p = 0. \tag{3.30}$$

The shear force is dominated by the contribution from region I, since the gap widens rapidly in region II. Since the pressure gradient in region I is negligible, the velocity profile in the gap is linear, and

$$F_\tau = 8\int_0^{\pi/2}\frac{U_p}{H_1(\theta)}R_1^2\cos^2\theta\,\mathrm{d}\theta. \tag{3.31}$$

The pressure force acting on the control volume is approximated by

$$F_p = -12R_2\int_{-\pi}^{\pi}P^{\mathrm{III}}(R_2,\theta)\cos\theta\,\mathrm{d}\theta = -12\pi R_2^2(1+R_2^{-2}a_1). \tag{3.32}$$

3.7. *Geometrical constraint on gap width*

The gap width depends on the surface area and volume of the cell, and on the spacing between the plates. When the spacing between the plates equals the width w_0 of the critical cell shape, the gap width must be zero. For slightly wider plate spacing, the constraints of fixed surface area and volume are applied approximately by specifying that the mean thickness of the cell in region I remains equal to w_0. The mean gap width therefore satisfies

$$H_{\mathrm{m}} = \frac{4}{\pi}\int_0^{\pi/2}H_1(\theta)\cos^2\theta\,\mathrm{d}\theta = \tfrac{1}{2}(1-\omega_0/d), \tag{3.33}$$

and using (3.28) and (3.29) we find that

$$U_{\rm p} H_{\rm m} = \frac{4}{\pi}\int_0^{\pi/2} Q_R^{\rm III}(R_2,\theta)\cos\theta\,{\rm d}\theta = U_{\rm p} - 1 + a_1/R_2^2. \tag{3.34}$$

3.8. *Asymptotic solution in the limit of small cell velocity*

To compute the cell shape and motion, equations (3.24), (3.29), (3.30) and (3.34) are solved for P_0, $U_{\rm p}$, the coefficients a_n and the function $H_1(\theta)$. First we assume that $U_{\rm p} \ll 1$, so that $a_1/R_2^2 \approx 1$ from (3.34). From (3.28) and (3.29), $a_n = O(U_{\rm p} H_{\rm m})$ for $n > 1$. Now, according to the scalings in §3.4, P_0 must be $O(H_{\rm m}^{-\frac{1}{3}})$, i.e. in this approximation, the pressure across the membrane is dominated by a large constant term, with an $O(1)$ term proportional to $\cos\theta$ and small corrections at higher angular frequencies. The gap width $H_1(\theta)$ is proportional to $|\cos\theta|^{\frac{2}{3}}$ and from (3.33), we obtain

$$H_1(\theta) = \frac{\pi H_{\rm m}|\cos\theta|^{\frac{2}{3}}}{4I(\frac{8}{3})} \quad \text{where} \quad I(\nu) = \int_0^{\pi/2}\cos^\nu {\rm d}\theta. \tag{3.35}$$

From (3.31),

$$F_\tau = (32/\pi)\,I(\tfrac{8}{3})\,I(\tfrac{4}{3})\,R_1^2\,U_{\rm p}/H_{\rm m} \tag{3.36}$$

and the zero-drag condition shows that

$$U_{\rm p} = \tfrac{3}{4}\pi^2 I(\tfrac{8}{3})^{-1} I(\tfrac{4}{3})^{-1}(R_2/R_1)^2 H_{\rm m} \approx 11.61\,(R_2/R_1)^2 H_{\rm m}. \tag{3.37}$$

In comparison, if uniform gaps with width $H_{\rm m}$ are assumed, the same analysis yields (3.37) with the numerical coefficient 12 in place of 11.61. Therefore, the non-uniformity of the gap has only a slight effect on the particle velocity.

The constant leading-order term P_0 in the pressure difference across the membrane may now be estimated. In (3.24), we replace $P^{\rm III}(R_2,\theta)$ by P_0, and substitute the estimates for $H_1(\theta)$ and $U_{\rm p}$ from (3.35) and (3.37), yielding

$$P_0 = -(\tfrac{1}{2}k_1)^{\frac{3}{5}}[\pi I(\tfrac{8}{3})]^{\frac{1}{5}} I(\tfrac{4}{3})^{-1}(R_2/R_1)^2 H_{\rm m}^{-\frac{1}{5}}. \tag{3.38}$$

For the typical red cell dimensions, $R_1 = 1.64$ and $R_2 = 2.10$, and (3.27) then gives

$$P^{\rm III}(R_2,\theta) = -2.92 H_{\rm m}^{-\frac{1}{3}} + 4.20\cos\theta + o(1), \tag{3.39}$$

confirming that the constant term is in fact dominant for small gap widths.

3.9. *Numerical solutions for finite cell velocities*

The large numerical coefficient in (3.37) implies that cell velocity increases rapidly with increasing gap width. Therefore, we may consider cases in which $H_{\rm m}$ remains small, about 0.1 for instance, but $U_{\rm p}$ is not small. If we assume that $U_{\rm p} = O(1)$, the scaling arguments in §3.4 yield almost the same equations as before, the only changes being that $U_{\rm t}$ is replaced with $U_{\rm p}$ and $\alpha_2 = \alpha_3 = -\frac{3}{2}$ instead of $-\frac{1}{2}$. The analyses in §§3.5–3.7 are unchanged. However, the approximations for a_n in §3.8 no longer apply, and (3.29) and (3.30) are solved numerically. Substituting (3.28) and (3.24) in (3.29) and integrating over $[0,\pi]$, we obtain

$$a_n' = \frac{k_1 U_{\rm p} R_2^{2n}}{(2n-1)\pi}\int_0^\pi \left|\frac{U_{\rm p}\cos\theta}{6P^{\rm III}(R_2,\theta)}\right|^{\frac{2}{3}} \cos\theta\cos(2n-1)\,\theta\,{\rm d}\theta, \tag{3.40}$$

where $a_1' = a_1 + R_2^2(U_{\rm p} - 1)$ and $a_n' = a_n$ for $n > 1$.

For values of $H_{\rm m}$ in this range, region II contributes significantly to the total shear force F_τ, leading to a modified zero-drag condition (cf. Halpern & Secomb 1991, §3.6).

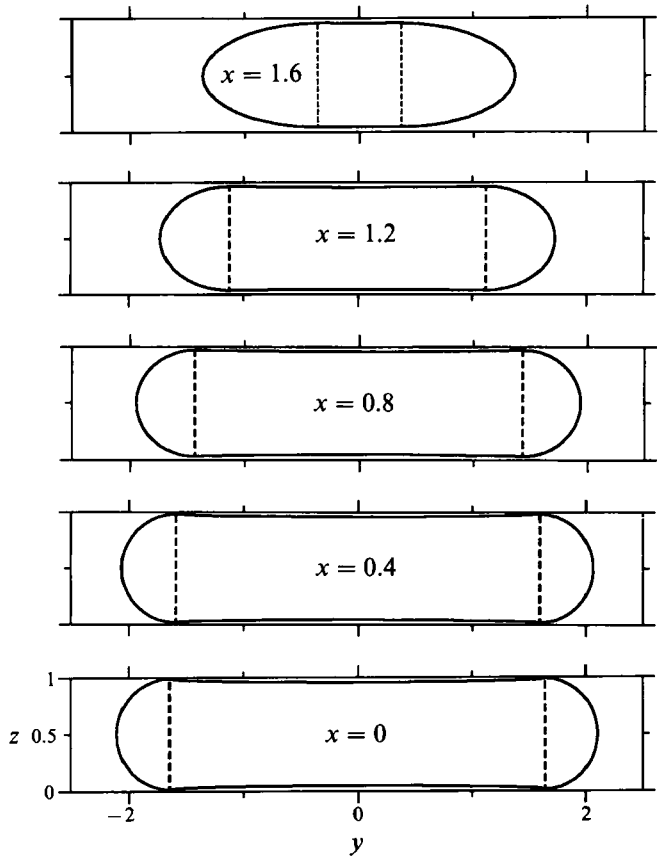

FIGURE 2. Cell shape at several cross-sections perpendicular to the flow direction, for the case $r_1 = 3.25$ μm, $r_2 = 4.16$ μm, $w_0 = 0.91$ μm, $d = 1.98$ μm.

Using (3.24), the shear force F_τ and the mean gap width H_m in the geometrical constraint (3.33) may be written in terms of integrals of powers of $P^{III}(R_2, \theta)$ and $\cos\theta$. We then use an iterative approach to solve (3.30), (3.32), (3.33) and (3.40) for P_0, U_p, H_m and a'_n. Initially, we assume that $a'_n \approx 0$ and solve the nonlinear system (3.30), (3.32) and (3.33) for P_0, U_p and H_m. Then we use (3.40) to compute new estimates for a'_n. This procedure is repeated until convergence is achieved.

Figure 2 shows the computed shape of the cell at several cross-sections perpendicular to the flow direction. For simplicity, only the shape in regions I and II is graphed. In region II, the rim is semicircular in profile, and oblique sections are obtained when $X > 0$. The location of the narrow transition region between regions I and II is indicated by a vertical dashed line. The gap width between the cell and the wall in region I is seen to decrease with distance from the axis of symmetry parallel to the flow direction.

Figure 3 shows the variation of U_p as a function of H_m, according to the theories of §§3.8 and 3.9. Corresponding results for a rigid particle with critical shape are included for comparison, from Halpern & Secomb (1991). The results for rigid and flexible particles do not differ appreciably, despite the other significant differences between the two cases. Cell velocity may be smaller or larger than mean bulk velocity depending on the spacing of the plates, with equality when the width of the cell is about 70% of the channel width. As the gap width increases, the asymptotic theory

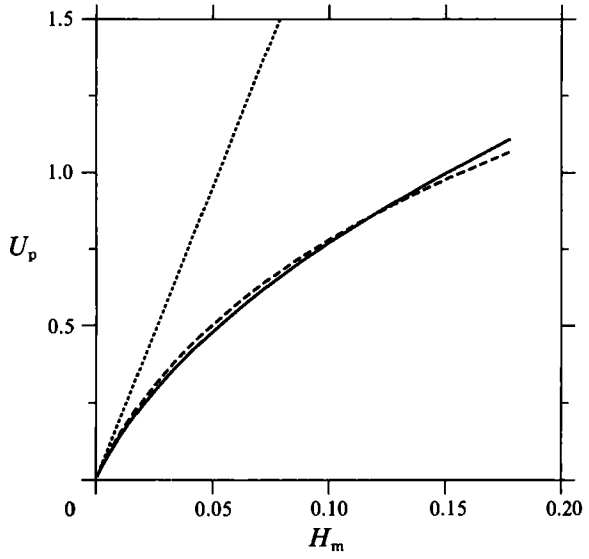

FIGURE 3. U_p as a function of H_m: —, flexible cell; – –, rigid particle of critical shape; - - -, asymptotic result in limit of small U_p. Values of r_1, r_2 and w_0 as in figure 2.

of §3.8 increasingly overestimates U_p, since it does not take into account the reduction of the driving pressure when the cell moves with the flow, or the contribution of region II to F_τ.

In this analysis, we have assumed that the overall shape of the cell in the (X, Y)-plane is circular. For very narrow gap widths, this is guaranteed by the constraints of surface area and volume, which dictate that the cell must remain close to its critical shape. As the gap width increases, for instance for values H_m of about 0.05, the geometrical constraints no longer guarantee that the shape is approximately circular. However, (3.39) shows that the pressure difference, and hence the membrane tension, still remains approximately uniform around the circumference of the cell for such gap widths. This uniform stress presumably tends to maintain the circular shape of the cell. Analysis of overall shape changes would require relaxation of some of the simplifications of the model, including the assumptions leading to (3.10).

For sufficiently large gap widths, the overall cell shape probably becomes significantly distorted, but the main features of the present analysis should still apply. For instance the conclusion that gap width is uniform in the flow direction in region I is independent of the shape of region I. Similarly, the equations presented in the next section concerning membrane strain in region I will still apply, and the qualitative behaviour will be similar. However, if the overall shape is distorted, the mean gap width H_m is necessarily smaller than the estimate (3.33), and so the particle velocity is lower than estimated above. In this case, the estimates shown in figure 3 would represent upper bounds.

4. Strain/stress analysis of region I

We next consider the membrane strains that will result from the fluid stresses implicit in the above analysis. For simplicity, we restrict our attention to region I, although membrane strain will also occur in region II.

4.1. *Membrane equilibrium*

Since the curvature is very small, we may treat the membrane as essentially two-dimensional. We define in-plane stress resultants $\kappa T_{11}, \kappa T_{22}$ and κT_{12}, where κ is the elastic modulus. The equations of membrane equilibrium are

$$\frac{\partial T_{11}}{\partial X_1}+\frac{\partial T_{12}}{\partial X_2}=-\frac{\epsilon}{H(X_2)}, \tag{4.1}$$

$$\frac{\partial T_{12}}{\partial X_1}+\frac{\partial T_{22}}{\partial X_2}=0, \tag{4.2}$$

where $H(X_2)$ is the gap width in region I, $(X_1, X_2) \equiv (X, Y)$ and $\epsilon = \mu u_1/\kappa$ is a ratio of viscous to elastic forces.

In analogous axisymmetric geometries, the fluid stresses can be balanced by isotropic membrane tension (Secomb *et al.* 1986; Halpern & Secomb 1989). Here, if we assume that the membrane stress is isotropic, i.e. $T_{11} = T_{22}$ and $T_{12} = 0$, then since $H(X_2)$ is not a constant, (4.1) and (4.2) are inconsistent. Therefore membrane equilibrium can only be achieved if shear resultants are generated.

4.2. *Constitutive relations for the membrane*

Consider a deformation in which the stretch ratios in principal axes are λ_1 and λ_2. We suppose that the corresponding membrane stresses in principal axes may be expressed in terms of a strain-energy function:

$$\kappa T_1^{\mathrm{p}}=\frac{1}{\lambda_2}\frac{\partial \omega}{\partial \lambda_1} \quad \text{and} \quad \kappa T_2^{\mathrm{p}}=\frac{1}{\lambda_1}\frac{\partial \omega}{\partial \lambda_2}. \tag{4.3}$$

Since membrane area is conserved, the constraint $\lambda_1\lambda_2 = 1$ must be imposed and an unknown isotropic stress T^0 (analogous to the hydrostatic pressure in incompressible flow) must be added. For consistency with Evans & Skalak (1980) and Secomb *et al.* (1986) we assume that $\omega = \frac{1}{2}\kappa(\lambda_1^2+\lambda_2^2)$, yielding

$$T_1^{\mathrm{p}}=\lambda_1^2+T^0 \quad \text{and} \quad T_2^{\mathrm{p}}=\lambda_2^2+T^0. \tag{4.4}$$

Other forms of strain-energy function for red cell membrane have been proposed (Skalak *et al.* 1973; Barthès-Biesel & Rallison 1981). All are equivalent for small strains.

For general deformations, let ξ be the position of a point of the membrane in the reference configuration, and label the corresponding point in the final configuration $\boldsymbol{X} = \boldsymbol{X}(\xi)$. Define the 2×2 relative deformation tensor

$$\boldsymbol{C}=\frac{\partial \boldsymbol{X}}{\partial \xi} \tag{4.5}$$

Then $\omega = \frac{1}{2}\kappa \operatorname{tr}(\boldsymbol{C}\cdot\boldsymbol{C}^{\mathrm{T}})$, and by a rotation from principal to coordinate axes, it is found (cf. Barthès-Biesel & Rallison 1981) that

$$\boldsymbol{T}=\boldsymbol{C}\cdot\boldsymbol{C}^{\mathrm{T}}+T^0\boldsymbol{I}. \tag{4.6}$$

4.3. *Small deformations*

First we consider the case of small membrane strains, for ϵ sufficiently small. Let

$$\boldsymbol{X}=\xi+\boldsymbol{\chi}(\xi) \quad \text{where} \quad \partial\boldsymbol{\chi}/\partial\xi \ll 1. \tag{4.7}$$

The condition of area conservation implies that $|\partial \boldsymbol{X}/\partial \boldsymbol{\xi}| = 1$, and so

$$\partial \chi_1/\partial X_1 + \partial \chi_2/\partial X_2 = 0 \tag{4.8}$$

and a function, ψ, may be introduced such that

$$\chi_1 = \partial \psi/\partial X_2, \quad \chi_2 = -\partial \psi/\partial X_1. \tag{4.9}$$

From (4.5) and (4.6), the stress is to leading order

$$T_{11} = 1 + 2\frac{\partial^2 \psi}{\partial X_1 \partial X_2} + T^0, \quad T_{22} = 1 - 2\frac{\partial^2 \psi}{\partial X_1 \partial X_2} + T^0, \quad T_{12} = \frac{\partial^2 \psi}{\partial X_2^2} - \frac{\partial^2 \psi}{\partial X_1^2}, \tag{4.10}$$

Substituting in the membrane equilibrium equations (4.1) and (4.2), and eliminating T^0, we find

$$\nabla^4 \psi = -\epsilon \, \partial H(X_2)^{-1}/\partial X_2. \tag{4.11}$$

Boundary conditions are obtained by considering the outer edge of the cell, $R = R_2$, which is located in the plane $Z = \frac{1}{2}$. By symmetry, there is no membrane displacement across this plane, and no membrane shear stress on it. Since the rim (region II) is relatively narrow compared to the radius of region I, and the shear stresses in region II are less than in region I, the same boundary conditions apply approximately at $R = R_1$. We therefore set

$$\psi = 0, \quad \frac{1}{R^2}\frac{\partial^2 \psi}{\partial \theta^2} - \frac{\partial^2 \psi}{\partial R^2} = 0 \quad \text{when} \quad R = R_1. \tag{4.12}$$

We seek a particular solution in the form $\epsilon g(X_2)$ where from (4.11),

$$g'''(X_2) = -H(X_2)^{-1}, \quad \text{i.e.} \quad g'''(R_1 \sin\theta) = -H_1(\theta)^{-1}. \tag{4.13}$$

From here on, we assume that $H_1(\theta)$ is given by (3.35), the result for small particle velocity U_p. The same procedure applies if U_p is not small, and an example is given by Halpern (1989). Integrating, we obtain

$$g''(R_1 \sin\theta) = -\frac{4I(\frac{8}{3})P_1}{\pi H_m}\int_0^\theta |\cos\Omega|^{\frac{1}{3}} \, d\Omega. \tag{4.14}$$

This may be expressed as a Fourier series:

$$g''(R_1 \sin\theta) = \sum_{k=1}^{\infty} b_k \sin(2k-1)\theta, \tag{4.15}$$

where

$$b_k = -\frac{16I(\frac{8}{3})R_1}{(2k-1)\pi^2 H_m}\int_0^{\pi/2} \cos^{\frac{1}{3}}\theta \cos(2k-1)\theta \, d\theta. \tag{4.16}$$

Equation (4.15) is integrated twice to yield

$$g(R_1 \sin\theta) = -\tfrac{1}{8}R_1^2 \sum_{k=1}^{\infty} c_k \sin(2k-1)\theta, \tag{4.17}$$

where $c_1 = b_1 + b_2, \quad c_k = \dfrac{b_{k-1}}{(k-1)(2k-1)} + \dfrac{b_k}{k(k-1)} + \dfrac{b_{k+1}}{k(2k-1)}$ for $k > 1$.

The solution of (4.11) and (4.12) is

$$\psi(R, \theta) = \epsilon[\psi_0(R, \theta) + g(R \sin\theta)] \quad \text{where} \quad \nabla^4 \psi_0 = 0, \tag{4.18}$$

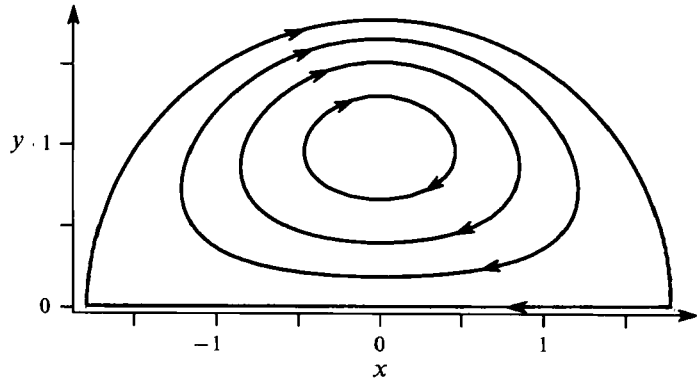

FIGURE 4. Membrane deformation in region I: contours of ψ. Values of r_1, r_2 and w_0 as in figure 2.

with boundary conditions at $R = R_1$:

$$\psi_0 = -g, \quad \frac{1}{R^2}\frac{\partial^2 \psi_0}{\partial \theta^2} - \frac{\partial^2 \psi_0}{\partial R^2} = \frac{\sin\theta}{R_1} g'(R_1 \sin\theta) - \cos 2\theta\, g''(R_1 \sin\theta). \tag{4.19}$$

The general solution to (4.18), with the required symmetry and finite at the origin, is

$$\psi_0 = \sum_{k=1}^{\infty} (A_k R^{2k-1} + B_k R^{2k+1}) \sin(2k-1)\theta. \tag{4.20}$$

Applying the boundary conditions (4.19) gives

$$A_k + R_1^2 B_k = \tfrac{1}{8} R_1^{3-2k} c_k \tag{4.21}$$

and

$$(2k-1)(4k-3) A_k + (8k^2 - 2k + 1) R_1^2 B_k = \tfrac{1}{8} R_1^{3-2k} d_k, \tag{4.22}$$

where $d_1 = 3b_2 - 5b_1$, $d_k = \dfrac{4k-3}{k-1} b_{k-1} + \dfrac{b_k}{k(k-1)} + \dfrac{4k-1}{k} b_{k+1}$ for $k > 1$.

The coefficients b_k are evaluated numerically, and A_k and B_k are obtained by solving (4.21)–(4.22).

Contours of ψ are plotted in figure 4. From (4.9), the displacement is parallel to the contours, and proportional to the density of contours. The membrane is dragged backwards at the extremities of the cell and moves forward on the centreline. Maximum displacement occurs at the extremities. Assuming typical values for shear elastic modulus, $\kappa = 0.0042$ dyn/cm, and plasma viscosity, $\mu = 1$ cP, and a mean gap width $H_m = 0.045$, the predicted maximum membrane displacement is about 1 μm when the cell velocity is 0.1 cm/s, and the maximum membrane stretch ratio is less than 1.2. Based on these estimates, the small-deformation theory is applicable for the above parameter values. At larger velocities, or smaller gaps, large deformations occur, but the membrane deformation is likely to be qualitatively similar.

It is interesting to note that the viscous resistance of the membrane to time-dependent deformation is analogous that of a viscous fluid to two-dimensional flow (Secomb & Skalak 1982), and is therefore governed by the equations as developed in this section, with the exception that the velocity replaces the displacement in (4.9), and the membrane viscosity replaces the elastic modulus. Consequently, figure 4 also depicts the streamlines of the membrane velocity which would occur if the same shear stress were applied suddenly to initially unstressed membrane to region I.

5. Discussion and conclusions

From this analysis, we may describe the shape of a tightly fitting red cell as it squeezes through the space between two parallel plates. The overall shape is a disk with almost flat faces (region I) and a curved rim (region II). A narrow transition region, in which pressure and membrane curvature vary rapidly, separates regions I and II. The gap width at the boundary of region I varies with circumferential position. At each point in the leading part of the boundary ($\frac{1}{2}\pi < |\theta| < \pi$), the gap width is uniquely determined by the local ratio of component of cell velocity to membrane tension. This gap width decreases towards the extremities of the cell ($\theta = \pm\frac{1}{2}\pi$).

Within region I, the pressure in the gap is approximately uniform. This contrasts with the results of Halpern & Secomb (1991) for rigid disk-shaped particles, in which large pressure gradients were predicted in region I for very narrow gaps. For flexible particles, the uniform pressure in the gap implies that the gap width is uniform in the direction parallel to the flow. This condition dictates the gap width at the trailing boundary of region I ($|\theta| < \frac{1}{2}\pi$). In the transition region, the gap width varies monotonically in the leading part of the cell, but oscillates in the trailing part.

Since the gap width in region I is not uniform, the fluid stresses on the membrane cannot be balanced by isotropic tension in the membrane. Shear stresses are generated within the membrane, which increase in proportion to flow velocity. Consequently, membrane shear strain must also increase with increasing flow velocity. This contrasts with the case of an axisymmetric cell in a cylindrical tube, in which in-plane membrane shear stress and strain remain bounded as cell velocity increases.

In cylindrical tubes, red blood cells travel faster than the mean bulk flow since they tend to travel along the axis of symmetry. Hence, the tube haematocrit (volume fraction of red cells) is always less than the discharge haematocrit (flow fraction of red blood cells). This is known as the Fahraeus effect. In channels, however, red cells can travel slower than the mean bulk flow if the gaps between the cell and the walls are narrow. In this case, 'tube' hematocrit H_T is elevated relative to discharge hematocrit H_D, according to the relation $H_T/H_D = U_p^{-1}$. The difference lies in the fact that in slots the suspending fluid can easily bypass the cell, so that the cell velocity can be much less than the mean bulk velocity. The variation of cell velocity with spacing of the walls for flexible particles is similar to that previously predicted by Secomb & Halpern (1991) for rigid disk-shaped particles of corresponding dimensions.

In summary, this analysis demonstrates two phenomena accompanying motion of red blood cells through narrow parallel-sided channels that are not present in axisymmetric tubes: an increase in local tube hematocrit relative to the discharge hematocrit; and the generation of shear stresses in the cell membrane, which increase unboundedly with increasing cell velocity. Both phenomena probably also occur in narrow pathways with other, more complicated non-axisymmetric geometries, such as are encountered by red blood cells in the microcirculation.

This work was supported by National Institutes of Health grants HL34555, HL17421 and HL07249, and has been performed in partial fulfilment of the requirements for the Ph.D. degree of D. Halpern at the University of Arizona.

REFERENCES

BARTHÈS-BIESEL, D. & RALLISON, J. M. 1981 The time-dependent deformation of a capsule freely suspended in a linear shear flow. *J. Fluid Mech.* **113**, 251–267.

CANHAM, P. B. & BURTON, A. C. 1968 Distribution of size and shape in populations of normal human red blood cells. *Circulation Res.* **22**, 405–422.

DRENCKHAHN, D. & WAGNER, J. 1986 Stress fibers in the splenic sinus endothelium in situ: molecular structure, relationship to the extracellular matrix, and contractility. *J. Cell Biol.* **102**, 1738–1747.

EVANS, E. A. & SKALAK, R. 1980 *Mechanics and Thermodynamics of Biomembranes.* Boca Raton, Florida: CRC Press.

FUNG, Y. C. 1990 *Biomechanics: Motion, Flow, Stress and Growth.* Springer.

GREENSMITH, J. E. & DULING, B. R. 1984 Morphology of the constricted arteriolar wall: physiological implications. *Am. J. Physiol.* **247**, H687–H698.

HALPERN, D. 1989 The squeezing of red blood cells through tubes and channels of near-critical dimensions. Ph.D. thesis, University of Arizona.

HALPERN, D. & SECOMB, T. W. 1989 The squeezing of red blood cells through capillaries with near-minimal diameters. *J. Fluid Mech.* **203**, 381–400.

HALPERN, D. & SECOMB, T. W. 1991 Viscous motion of disk-shaped particles through parallel-sided channels with near-minimal widths. *J. Fluid Mech.* **231**, 545–560.

SECOMB, T. W. & SKALAK, R. 1982 Surface flow of viscoelastic membranes in viscous fluids. *Q. J. Mech. Appl. Maths* **35**, 233–247.

SECOMB, T. W., SKALAK, R., ÖZKAYA, N. & GROSS, J. F. 1986 Flow of axisymmetric red blood cells in narrow capillaries. *J. Fluid Mech.* **163**, 405–423.

SKALAK, R., TOZEREN, A., ZARDA, R. P. & CHIENS, S. 1973 Strain energy function of red blood cell membranes. *Biophys. J.* **13**, 245–264.

TIMOSHENKO, S. & WOINOWSKY-KRIEGER, S. 1959 *Theory of Plates and Shells.* McGraw-Hill.